ABSTRACT

Title of Document: **EARTH ABUNDANT BIMETALLIC NANOPARTICLES FOR HETEROGENEOUS CATALYSIS**

Jonathan F. Senn, Jr., Master of Science, 2014

Directed By: Professor, Bryan Eichhorn
Department of Chemistry and Biochemistry

Polymer exchange membrane fuel cells have the potential to replace current fossil fuel-based technologies in terms of emissions and efficiency, but CO contamination of H_2 fuel, which is derived from steam methane reforming, leads to system inefficiency or failure. Solutions currently under development are bimetallic nanoparticles comprised of earth-abundant metals in different architectures to reduce the concentration of CO by PROX during fuel cell operation. Chapter One introduces the Pt-Sn and Co-Ni bimetallic nanoparticle systems, and the intermetallic and core-shell architectures of interest for catalytic evaluation. Application, theory, and studies associated with the efficacy of these nanoparticles are briefly reviewed. Chapter Two describes the concepts of the synthetic and characterization methods used in this work. Chapter Three presents the synthetic, characterization, and catalytic findings of this research. Pt, PtSn, $PtSn_2$, and Pt_3Sn nanoparticles have been synthesized and supported on γ-Al2O3. Pt_3Sn was shown to be an effective PROX catalyst in various gas feed conditions, such as the gas mixture incorporating 0.1% CO, which displayed a light-off temperatures of ~95°C. Co and Ni monometallic and CoNi bimetallic nanoparticles have been synthesized and characterized, ultimately leading to the development of target Co@Ni core-shell nanoparticles. Proposed studies of catalytic properties of these nanoparticles in preferential oxidation of CO (PROX) reactions will further elucidate the effects of different crystallographic phases, nanoparticle-support interactions, and architecture on catalysis, and provide fundamental understanding of catalysis with nanoparticles composed of earth abundant metals in different architectures.

EARTH ABUNDANT BIMETALLIC NANOPARTICLES FOR HETEROGENEOUS CATALYSIS

By

Jonathan F. Senn, Jr.

Thesis submitted to the Faculty of the Graduate School of the
University of Maryland, College Park, in partial fulfillment
of the requirements for the degree of
Master of Science
2014

Advisory Committee:
Professor Bryan Eichhorn, Chair
Professor Efrain Rodriguez
Professor Andrei Vedernikov

Dedication

To my parents Jonathan Senn, Sr. and Glynis Senn, my brother, my grandparents, my friends, my family, and Darian Scott-Carter.

Acknowledgements

I would like to thank my advisor, Professor Bryan Eichhorn for all of the guidance and support that I have received throughout my graduate career. You helped transform my varied undergraduate research experiences into professional-leveled characteristics that will serve as a basis throughout my professional career.

I would like to thank the members of the Eichhorn group for the friendship that we have shared during our time in graduate school. The joint projects and mutual support that we have shared has been invaluable to my experiences.

I would especially like to thank Chris Sims for his mentorship throughout this entire process. Without your guidance, encouragement, and desire to see me succeed, I would not have been able to reach my full potential as a graduate-leveled chemist.

My undergraduate research advisors and professors at Carnegie Mellon University that have given me the confidence and technical skills to reach this point in my professional career also deserve recognition: Dr. Greg Rohrer, Dr. Susan Graul, Dr. Stefan Bernhard, and Ms. Karen Stump. The vigor, exuberance, and positivity that you embodied have and continue to sustain me in my chemistry and materials science interests.

To my friends, thank you for the fun times and the encouragement that have nourished me throughout this journey. As we continue to watch each other grow, our bonds deepen and I would be lost without you. To my best friend, you have seen me through the ups and the downs, and you have always kept me on the path of enlightenment and happiness. You always remind me that there is so much to life, and that it is ours for the taking. May we always aim for our dreams, and push each other to reach the stars, as we have done in past years.

Another person central to this achievement is Darian Scott-Carter, a person of strength, integrity, and perseverance. You have helped me learn numerous life-lessons in these formative years, and you arrived in my life at a very serendipitous and crucial moment. I will never forget the fun, kindness, and journey that we have shared thus far, and will continue to share.

Lastly, my mother, my father, my brother, my loving grandparents, and my family have all been integral to my life-long development. The love, support, and constant curiosity into my research never cease to amaze me! I have achieved many things in my life, and I will continue to strive for my dreams, but without you, none of this would be possible. They say it takes a village to raise a child; well, I'd say my village has done an exceptional job, and I love you for it.

Table of Contents

List of Schemes

Chapter 1

Chapter 2

Chapter 3

List of Figures

Chapter 1

Chapter 3

List of Abbreviations

Å	Angstrom
μL	microliter
μM	micromolar
σ_g	Sigma gerade
acac	Acetylacetonate
At %	Atomic percent
°C	Degrees Celsius
cm^{-1}	wavenumber
Co@Ni	Cobalt Nickel core-shell alloy
DFT	Density functional theory
DMFC	Direct methanol fuel cell
DPE	Diphenyl ether
E_F	Fermi energy level
EDX	Energy dispersive X-ray
EG	Ethylene glycol
eV	Electron volts
g	Grams
GADDS	General area diffraction detection system
GC	Gas chromatography
GHSV	Gas hourly space velocities
h	hour
HDD	1,2-hexadecanediol

HRTEM	High resolution transmission electron microscopy
IR	Fourier-transform infrared spectroscopy
K	Kelvin
M	molar
mA	Milliamps
mg	Milligram
mL	Milliliter
mM	millimolar
mV	millivolts
min	minute
MW	Molecular weight
nm	nanometer
NP	nanoparticle
PGM	Platinum group metal
ppm	Parts per million
$Pt(acac)_2$	Platinum acetylacetonate
PtSn@Sn	Platinum Tin – Tin sore-shell slloy
PEMFC	Polymer exchange membrane fuel cell
PROX	Preferential oxidation of carbon monoxide
PSA	Pressure-swing adsorption
PVP	Polyvinyl pyrrolidone
rpm	rotations per minute
RT	Room temperature

SMR	Steam methane reforming
Sn@Pt	Tin Platinum core-shell alloy
STEM	Scanning transmission electron microscopy
TCD	Thermal conductivity detector
TEM	Transmission Electron Microscopy
UHP	Ultra high purity
WGS	Water-gas shift
Wt %	Weight percent
XRD	Powder X-ray diffraction

Chapter 1: Heterogeneous Catalysis using Earth-Abundant Nanoparticles

1.1 Polymer Exchange Membrane Fuel Cells and Preferential Oxidation of CO

Environmental and economic influences have lead to the advancement of alternative energy technologies, such as proton exchange membrane fuel cells (PEMFC).[1] These fuel cells convert chemical energy into electrical energy for stationary and portable fuel cells applications, such as vehicles. Oxidation at the anode splits H_2 into protons and electrons, which transfer to the cathode via the polymer electrolyte membrane and the load circuit, respectively, and combine with O_2 through a reduction reaction. The PEMFC does not release greenhouse gases or pollutant emissions, only water and heat, possibly serving as an alternative to current combustion-based technologies. One of the limitations that prevent broader commercialization of this technology is the purity of hydrogen fuel for the anodic processes of the fuel cell. Currently, ~95% of industrial hydrogen in the US is produced by steam methane reforming (SMR) (eq 1).[2] Resultant syn-gas contains H_2 and CO, which poisons the anodic catalyst of the PEMFC, causing an increase in the overpotential of the hydrogen oxidation reaction[3]. Industrial applications typically remove CO from syn gas in two steps: 1. The water-gas shift (WGS) reaction (eq. 2); and 2. Purification by pressure-swing adsorption (PSA) or membrane reactor.[4,5] Preferential oxidation of CO (PROX) (eq. 3) is a smaller scale, alternative purification technique to reduce the CO concentration below 10 ppm, which is necessary for stable PEMFC

operation.[3] Theoretical and experimental studies have evaluated monometallic, bimetallic, and other catalytic systems for activity and selectively for the PROX reaction to improve economic viability of the PEMFC.[2,6-11]

$$CH_4 + H_2O \longrightarrow CO + 3H_2 \quad (1)$$

$$H_2O + CO \longrightarrow CO_2 + H_2 \quad (2)$$

$$1/2O_2 + H_2 + CO \longrightarrow CO_2 + H_2 \quad (3)$$

Platinum group metals (PGM) are common catalysts, but expense and rarity severely limit the commercial viability of the PROX and PEMFC system.[6] Findings have shown that PGMs combined with earth abundant metals exhibit comparable or superior PROX activity in comparison to commonly used Pt supported on γ-Al_2O_3.[7,12-16] Reducing or removing PGMs can reduce the cost and increase the activity of PROX catalysts.

1.2 Kinetics of Nanoparticle Formation

Finke and coworkers pioneered kinetic studies of transition metal nanoparticle (NP) formation, and derived mechanisms from kinetic and spectroscopic data;[17-21] they have shown that NPs form through a series of steps: 1. Slow, continuous nucleation of metal atoms from metal precursors; 2. Autocatalytic surface growth, where metal precursors are converted into surface atoms on NPs[17]; 3. Diffusive agglomerative growth of NPs to form bulk metal particles[20]; and 4. Autocatalytic agglomeration of NPs and bulk metal (scheme 1-1).[19] In addition, dissolution of smaller nuclei and the re-deposition of these atoms on larger nuclei in order to reduce surface energy, is another widely accepted mechanism known as Ostwald ripening.[22] There are many other theories and kinetic studies on homogeneous nanoparticle formation, however, the aforementioned are considered major benchmarks in nanoparticle growth.[21,23]

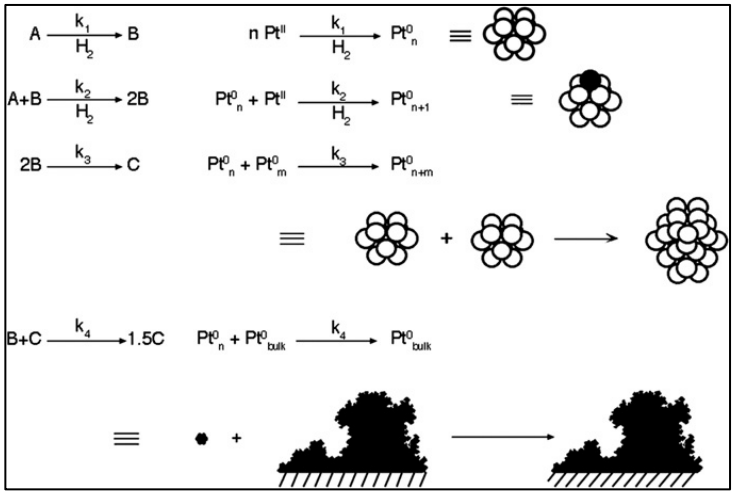

Scheme 1-2. Illustration of the 4-step mechanism of transition-metal nanoparticle formation proposed by Finke and coworkers. Figure taken from reference 8.

1.3 Bimetallic Nanoparticles

1.3.1 Bimetallic Nanoparticle Architectures

Bimetallic NPs exist in the following architectures: heteroaggregate, random alloy, intermetallic, and core-shell (fig. 1-1). Heteroaggregates consist of two types of NPs linked through physical or chemical interactions.[24] Random alloys have metals distributed randomly on lattices resembling parent metals. Conversely, intermetallics have distinct phases with well-defined lattices.[16] The structure of a core-shell is a core of metal or metal oxide covered by a layer, or shell, of a second metal.[25] Each architecture exhibits advantages and disadvantages in stability and catalytic activity.

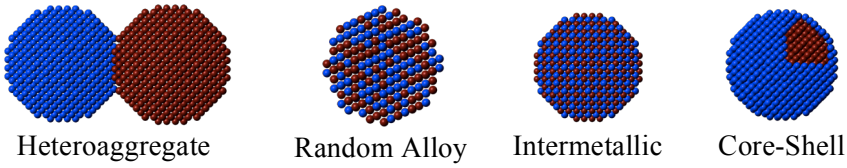

Figure 1-1. Bimetallic nanoparticle architectures (left to right): heteroaggregate, random alloy, intermetallic, and core-shell

Synergistic effects of surface metal species in intermetallics have been studied. Direct methanol fuel cell (DMFC) electrooxidation experiments by Gasteiger and co-workers showed CO to linearly adsorb to electron rich Pt (eq. 4), while adjacent Ru binds the oxygen-based species (eq. 5) that migrates and oxidizes CO to CO_2 (Eq. 6).[26,27] This bifunctional mechanism lowers the potentials necessary for CO electrooxidation on Pt-Ru alloy in comparison to monometallic Pt, similar to the decrease in thermal energy required for CO oxidation in Pt-Ru PROX studies.[25] In addition, Aricò and co-workers proposed that Pt-Sn alloys exhibit charge transfer from Sn to Pt[28], increasing free, active Pt sites by promoting adsorption of oxygen-based species on electron poor Sn.[9,28,29] Random alloys can also benefit from synergistic effects, however intermetallics have superior behavior due to increased stability and lack of isolated segregation of surface metal atoms[16].

$$\text{Pt-CH}_3\text{OH}_{\mathbf{ads}} \longrightarrow \text{Pt-CO}_{\mathbf{ads}} + 4\text{H}^+ + 4\text{e}^- \quad (4)$$

$$\text{Ru} + \text{H}_2\text{O} \longrightarrow \text{Ru-OH}_{\mathbf{ads}} + \text{H}^+ + \text{e}^- \quad (5)$$

$$\text{Pt-CO}_{\mathbf{ads}} + \text{Ru-OH}_{\mathbf{ads}} \longrightarrow \text{Pt} + \text{Ru} + \text{CO}_2 + \text{H}^+ + \text{e}^- \quad (6)$$

1.3.2 Electronic Effects of Core-Shell Architectures

DTF studies on the influence of d-band orbitals on molecular adsorption were pioneered by Norskøv and Hammer in development of the d-band theory[11,30-32]. Orbitals available for binding are adsorbate dependent; H_2 adsorption uses H 1s orbitals, while CO adsorption occurs via the 5σ and $2\pi^*$ orbitals through hybridization with metal d-orbitals. (fig 1-2).[11,29]

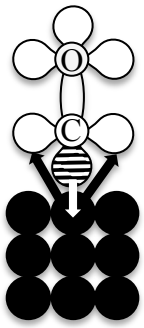

Figure 1-2. Graphical representation of CO 5σ (shaded) donation to the Pt surface (black), and back donation from the Pt surface to the CO 2π* orbital; the latter interaction has a greater influence on binding behavior. Figure adapted from reference 29.

The position of the d-band center, relative to the Fermi level, determines the position of the surface-adsorbate hybridized orbitals. For instance, a d-band center relatively higher in energy can produce a hybridized antibonding state above the Fermi level, forcing electrons to occupancy the bonding orbital below the Fermi level; stronger chemisorption is observed due to bonding orbital occupancy and an unfilled antibonding orbital. Conversely, relatively lower d-band center results in occupation of the bonding and antibonding orbitals, weakening chemisorption.[11,31] This exemplifies the effect of position of the d-band center on degree of filling of hybridized orbitals, and subsequent effect on chemisorption profile.

Substrate heteroatoms can alter d-band center position, affecting the chemisorption of adsorbate molecules and catalytic activity[10,33]. Theoretical studies have shown that d-band shifts depend on architecture and the alloyed elements[32]. Experimental catalytic studies of random alloy and intermetallic NPs confirm theoretical findings on d-band shifts, demonstrated by the d-band shift of monometallic Pt compared to Pt in Cu_3Pt (fig. 1-3)[34-36]; however, charge transfer effects play a greater role in the catalytic observations for this architecture.

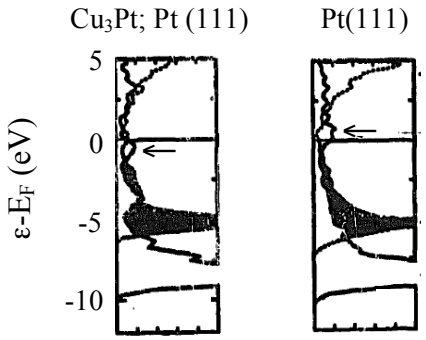

Figure 1-3. Density of states diagram of H_2 adsorbed to (a) Pt (111) in Cu_3Pt and (b) Pt (111) monometallic sites. Arrows indicate hybridized (σ_g – d) antibonding states. Relative to the Fermi level (ε-E_F = 0 eV; solid black, horizontal line), the lower antibonding orbital of Cu_3Pt confers weaker hydrogen chemisorption. Figure taken from reference 30.

Surface atoms of core-shell systems also exhibit d-band shifts, but with greater implications towards tailoring of catalytic properties (fig. 1-4)[34]. In work by Eichhorn and co-workers, Ru@Pt core-shell NPs are able to oxidize CO to CO_2 in contrast to typical CO poisoning of Pt surfaces.[25] Electron poor core Ru atoms draw electron density from surface Pt atoms, causing the Pt d-band center to shift lower in energy[6]. Finally, core-shell NPs allocate catalytically active atoms exclusively to the surface, requiring precious metal content only for catalysis, not bulk NP formation.

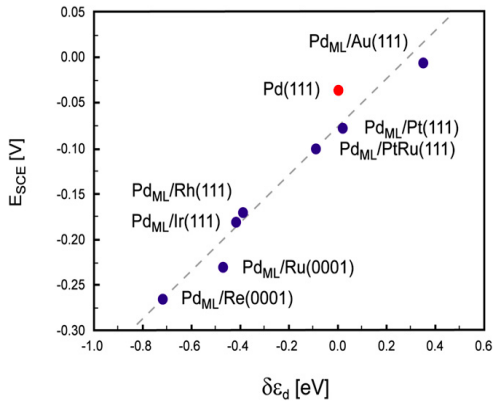

Figure 1-4. Electrochemically measured chemisorption energies of hydrogen on various Pd-based surfaces correlated to calculated shifts of the d-band center. Figure taken from reference 29.

Decreasing the cost of NPs by reducing Pt content and replacing Pt with earth abundant metals is possible using intermetallic and core-shell bimetallic architectures. Aforementioned bimetallic studies have shown that catalytic activities for these types of proposed NPs are comparable to commonly used NP catalysts. Theoretical studies have surveyed various monometallic and bimetallic surfaces to predict electronic and catalytic properties. Herein, Pt-Sn and Co-Ni NP systems have been synthesized, characterized, and analyzed for catalytic activity to investigate the efficacy of these NPs in an effort to increase viability and abundance in commercial applications.

1.4 Bimetallic Systems of Interest

1.4.1 Pt-Sn Bimetallic Nanoparticle System

The landmark bimetallic Pt-Sn system study by Gasteiger and co-workers investigated the electrochemical oxidation of CO and a H_2/CO mixture by bulk Pt_3Sn, and compared subsequent results to previous studies of bulk PtRu.[9,37,38] As mentioned previously, selective adsorption of CO and O_2 in the Pt-Sn system provides exceptional catalytic activity through the bifunctional mechanism.[9] The intermetallic phases PtSn, Pt_3Sn, and $PtSn_2$ have been synthesized and analyzed for catalytic activity in H_2 oxidation and PROX.[16,39,40] The investigation of support-catalyst interactions on thermal PROX activity for different Pt-Sn phases is the objective of this comparative study.

1.4.2 Co-Ni Bimetallic Nanoparticle System

D-band theory and DFT calculations (fig. 1-5) predict a down-shift of the d-band center of Ni in Co@Ni, resulting in lower CO and H_2 binding energies[32], and good catalytic activity comparable to other catalysts. Monometallic Co and Ni NPs are

catalytic materials commonly used in applications such as Fischer-Tropsch reactions[44-47] and dehydrogenation reactions[48-52]. Co-Ni bimetallic NPs have minimal synthetic and characteristic studies, and lack catalytic studies, allowing further evaluation of the system.[53-56] The Co-Ni phase diagram illustrates thermodynamic restriction to form only the random alloy. Novel synthesis of new Co-Ni core-shell variations will require rigorous air-free synthesis to prevent the formation of Ni oxide or Co oxide compounds. Although these bimetallic NPs may have slightly lower catalytic activities compared to Pt-based catalysts, cost normalization in relation to catalytic activity could promote the commercial application of the much cheaper, completely earth abundant catalytic materials.

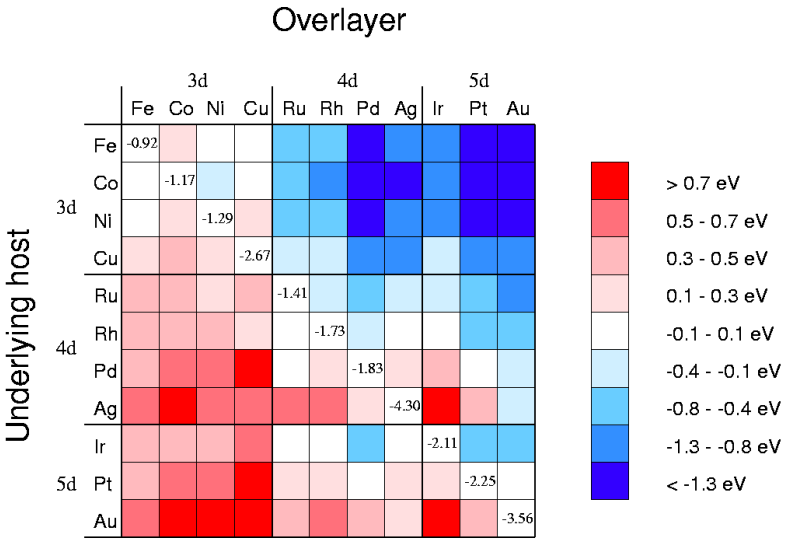

Figure 1-5. Shifts in d-band center of core-shell architectures relative to monometallic metal surface. Underlying host is the core and overlayer is the shell. Figure taken from ref. 27.

Based on experimental and theoretical studies, Pt-Sn and Co-Ni intermetallic and core-shell NPs have been synthesized, characterized, and analyzed for catalytic activity of the PROX reaction. Incorporating earth abundant metals in catalysts for PEMFC applications will encourage the economic viability and ubiquity of this technology.

Chapter 2: Synthesis and Characterization of Pt-Sn and Co-Ni Bimetallic Nanoparticles

2.1 Introduction

Described herein are the methods and theory of synthetic and characterization procedures necessary to achieve the goals of this research, as presented in Chapter One. Mechanisms of NP formation, development of different bimetallic architectures, and methods for supported catalysis synthesis are discussed in Chapter Two. Also, information necessary to catalytic analysis of supported NPs is presented in this Chapter.

2.2 Nanoparticle Synthesis

2.2.1 Reduction

The most common chemical route to form metal atoms in solution is the reduction of soluble metal salts and precursors. NPs in various architectures and compositions have been synthesized by reduction reactions using diols.[6,16,53,67,68] The mechanism of polyol reduction using ethylene glycol (EG) results in CO_2, aldehydes, and carboxylic acids as by-products of H-abstraction and electron transfer (scheme 2-1).[67] Synthesis of Pt monometallic and various core-shell NPs in this research employed this reduction reaction due to the high boiling point and efficient reducing ability of polyols, as well as facile removal from synthesized colloids.[16] Air-free and water-free reaction conditions were necessary for earth abundant nanoparticle synthesis to prevent unwanted oxidation, prompting the use of solid 1,2-hexadecanediol in organic solvents such as diphenyl ether (DPE) and 1-octadecene, as seen in Co-Ni bimetallic synthesis. [53,69]

Scheme 2-1. Ethylene glycol oxidation in the polyol reduction method of nanoparticle synthesis. Adapted from ref. 13.

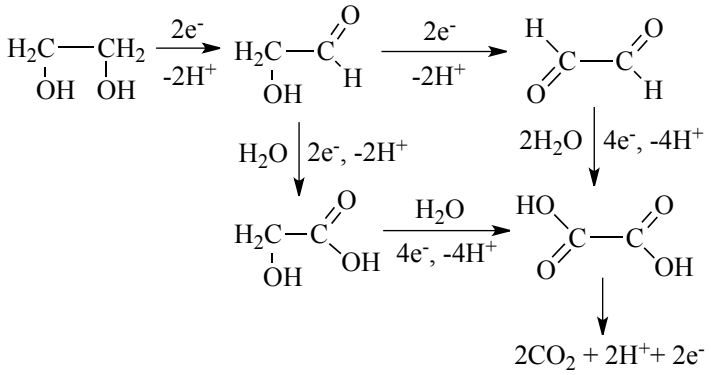

Strong reducing agents were also used in NP synthesis, as explored below. $NaBH_4$ reduction reactions[70,71] occur by hydride donation from BH_4^- to the metal precursor. Air-free reaction conditions, co-reduction of metal precursors, and the use of metal precursors with significantly negative reduction potentials[16] can require more reactive variations of $NaBH_4$, including superhydride[16,72], aluminum alkyls[70], and tetraalkylammonium hydrotriorganoborates.[73,74] Known as superhydride, $LiEt_3BH$[72] is much more reactive than $NaBH_4$ due to the electron donation from the ethyl groups to the boron, weakening the B-H bond and increasing hydritic character. The slightly less reactive analogue, $NaEt_3BH$, sufficed as the reducing agent in the Pt-Sn intermetallic[16] syntheses to simultaneously reduce these metallic species that have significant differences in standard reduction potentials.[107] These reductions used 1-octadecene and DPE as solvents due to violent reaction of $NaEt_3BH$ with water, which is prevalent in hydrophilic EG[75].

2.2.2 Core-Shell Formation

Core-shell preparation required greater consideration of synthetic techniques compared to random alloy and intermetallic syntheses. There are various routes to produce core-shells, but the following were of interest to this research: 1. Sequential

deposition, which can be epitaxial[76] or non-epitaxial[77], where core NPs are first generated, then shell atoms of another metal are deposited on the core[25,78,79]; 2. Redox transmetalation, where metal precursor material is introduced to core NPs, causing chemical reduction of the metal precursor due to lower reduction potential of core atoms[80,81]; and 3. Adsorbate induced surface segregation, where a random alloy or intermetallic is exposed to an adsorbate, and strong surface-adsorbate interactions cause one metal to migrate to the surface.[14,16,82,83] Core-shell synthesis focused on thermal reaction conditions, eliminating electrochemical variations of aforementioned methods.

Constituent metal properties are the bases for determining proper synthetic procedures. Co@Ni NPs were synthesized only using method 1 since Ni and Co have similar reduction potentials, -0.25 V and -0.28 V, respectively. Electrochemical CO-induced segregation has been used to produce PtSn@Sn NPs[16], but stability and size control of Sn NPs prevent the direct synthesis of the Sn@Pt NPs[84-86]. Regardless of synthetic procedure, NP stability is paramount to catalysis.

2.2.3 Surfactants

Finke and coworkers[87] investigated surfactants for transition-metal NPs based on electrostatic repulsion and steric hindrance properties that promoted kinetic control of NP formation, and prevented NP agglomeration.[87,88] Synthetic conditions and NP stability also influence surfactant choice. In this study, polyol syntheses used labile polyvinylpyrrolidone (PVP, MW=55,000) due to excellent solubility in these solvents. $NaEt_3BH$ reduction reactions in organic solvents used tightly binding surfactants, such as oleic acid, oleylamine and/or trioctylphosphine, which were necessary to prevent surface

oxides on earth abundant metal NPs.[89] While strong binding surfactants are difficult to remove before catalysis[79,88], researchers have investigated converting the surfactants into other compounds[88,90], sonication and centrifugation[6,91], and annealing procedures.[16] Lastly, strongly binding surfactants may inhibit shell growth on core NPs in core-shell syntheses. Surfactant-reaction pairings were made on the basis of literature and empirical findings.

2.2.4 Deposition on Support Materials

The final step to sample preparation was the deposition of NPs on a high surface area support material to effectively disperse the NPs, thereby reducing agglomeration and optimizing active sites available for catalysis.[18,74] Interactions between NPs and some support materials are also known to increase catalytic activity. Carbon black (Vulcan) has been used in countless electrochemical studies because of good electrical conductivity, pore size, and surface area.[92-94] In comparison to Vulcan, Graphene is used for increased conductivity and stability,[95,96] where nitrogen[97] or boron[96] can be dopants to further improve various properties. Thermal processes commonly use metal oxides such as γ-Al_2O_3 as support materials for stability and pore size as well[98], but the promotional effects of metal oxides on thermal catalysis have not been fully studied.[99] This study used impregnation methods to deposit NPs on support materials.[99] In addition, maximum catalytic activity with minimal loading of 1 wt % of NPs on support materials was implemented in order to decrease cost associated with catalytic material.

2.3 Characterization and Catalytic Analysis

Characterization of supported and unsupported NPs provided a scientific basis for observed properties and phenomena. Powder X-ray diffraction (XRD) was the preliminary technique used to identify crystal structure and architecture. Transmission electron microscopy (TEM) was used for size and shape analysis, while high resolution TEM (HRTEM) provided more details of NP surfaces. Energy dispersive X-ray spectroscopy (EDX), accessible in scanning transmission electron microscopy (STEM) mode[79], provided approximate analysis of elemental composition of NPs. The Fourier-Transform Infrared spectroscopy (IR) CO probe technique was used to observe core-shell growth, and distinguish random alloys and intermetallics from core-shell NPs due to energy differences in surface-CO interactions.[2,6,25,100-102]

Catalytic tests used 100 mg of NP-support material (ie. 1 wt% PtSn on γ-Al_2O_3) and occurred in a quartz fixed-bed flow-through reactor with an inner diameter of 6.8 mm. The reactor bed composition was the following: 600 mg quartz sand and 40 mg of quartz wool for gas homogenization; evenly loaded catalyst; then, additional quartz wool and quartz sand for support. Temperature was monitored and controlled with a K-type thermocouple in conjunction with Lab View software. Total flow rate and inlet velocities were chosen to be similar to previous studies for proper comparison.[6,25]. Outlet of the reactor was monitored by a Varian Chrompack CP-3800 gas chromatograph (GC) equipped with a thermal conductivity detector (TCD). This catalysis rig set-up and settings were inspired by previous studies.[6,25]

Catalytic reactions used various ultra high purity (UHP) feed gases and temperature profiles. Samples for PROX analysis were pretreated in flowing H_2 and He at

250°C, and tested in flowing H_2 and O_2, as well as CO in concentrations of 0.1%, 0.2%, and 1% balanced by He, and heated to 250°C.[6] Catalytic analysis was used to determine the efficacy of catalysts in terms of light-off temperature and selectivity for PROX. The primary goal for these catalytic studies was the observation and explanation of the relationship between catalytic activity and NP structure and architecture.

The objectives of this research were synthesis and characterization of Pt-Sn and Co-Ni NPs, and catalytic evaluation. Different Pt-Sn phases on different support materials were compared to the commercial standard Pt on γ-Al_2O_3. Co-Ni NPs may exhibit lower catalytic activity compared to Pt-Sn, but this new investigation into thermal catalysis using Co-Ni may show comparable catalytic activities that can be normalized by the decreased costs of these earth abundant metals. Theory and literature supporting these hypotheses and rationales are outlined in the introduction.

Chapter 3: Synthetic and PROX Analysis of Pt-Sn and Co-Ni Nanoparticles

3.1 Introduction

Chapter Three introduces the synthetic work and catalytic analyses performed in this research. Intermetallic and monometallic NPs composed of Pt-Sn and Co-Ni were synthesized by methods reported herein. XRD and TEM were used for characterization. Catalytic analysis of activity for the PROX reaction was investigated using PtSn and Pt_3Sn NPs supported on γ-Al_2O_3. Representative synthetic and characterization methods are presented, and detailed information can be found in the Supplemental Information section.

3.2 Pt-Sn Nanoparticles

3.2.1 Synthesis and Characterization

Intermetallic PtSn (1:1 ratio) with average diameter of 2.3 nm were synthesized by methods developed by Eichhorn and coworkers[16]. Co-reduction of $Pt(acac)_2$ and 47.6 mM $SnCl_4$ – heptane solution (1:1 molar ratio) in octadecene proceeded by hot injection of metal precursor solution into $NaEt_3BH$ – Octadecene solution at 190°C, using oleic acid and oleylamine. As-prepared NPs were deposited on γ-Al_2O_3 and annealed at 400°C to remove surfactants and attain intermetallic PtSn phase. TEM images show monodisperse PtSn NPs, as well as agglomerates (fig. 3-1a). Analysis of lattice fringes in HRTEM showed d-spacings of ~2.1 Å (fig. 3-1b) of the (102) plane of hexagonal

(*P6₃/mmc*) intermetallic PtSn. EDX data indicated an approximate 1:1 ratio of Pt and Sn atoms. The XRD profile of intermetallic PtSn also showed the hexagonal phase (fig. 3-2).

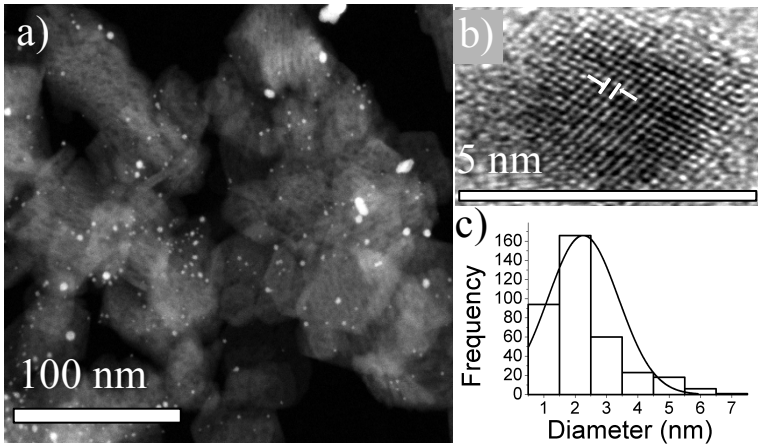

Figure 3-1. (a) Dark-field TEM image of 2.2 nm PtSn NPs supported on γ-Al_2O_3. (b) HRTEM image of PtSn NP supported on γ-Al_2O_3 with visible lattice fringes. (c) Histogram of NP size distribution.

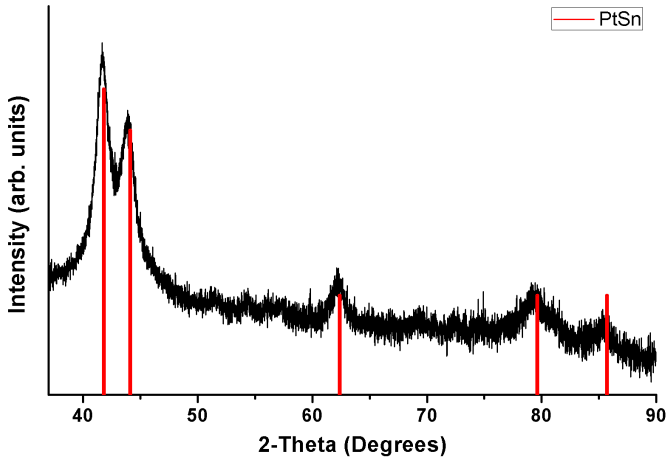

Figure 3-2. Powder XRD diffraction pattern of 2.41 nm intermetallic PtSn NPs supported on XC-72 vulcan (carbon black). JCPDS peak positions for PtSn are also displayed.

Synthesis of $PtSn_2$ and 3.9 nm Pt_3Sn intermetallics used methods similar to PtSn synthesis, with appropriate Pt and Sn precursor ratios.[39] XRD data of $PtSn_2$ supported on XC-72 Vulcan (carbon black) show the presence of minimal PtSn (fig. 3-3). TEM and EDX analysis of $PtSn_2$ on γ-Al_2O_3 showed exclusive formation of $PtSn_2$ in the analyzed

area (fig. S7-S8). Abundance of PtSn in $PtSn_2$ appears to differ with support material, possibly due to pore size differences.

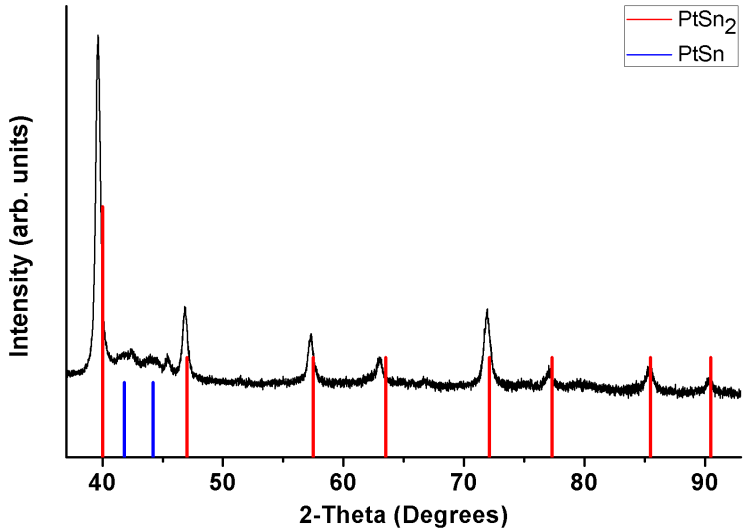

Figure 3-3. Powder XRD profile of 7.5 nm intermetallic $PtSn_2$ NPs supported on XC-72 vulcan (carbon black). Intermetallic PtSn NPs are present in the sample at ~33%, calculated in conjunction with Rietveld refinement. JCPDS peak positions for $PtSn_2$ are also present.

Synthesis of monometallic Pt NPs with an average diameter of 4.0 nm was performed via EG polyol reduction at 130°C, using $PtCl_2$ and PVP (MW=55,000).[105] As-prepared, unsupported NPs with a relatively small size distribution exhibit lattice fringes of ~2.3 Å, indicative of the (111) plane of cubic ($Fm\bar{3}m$) Pt, also confirmed by XRD.

3.2.2 PROX Analysis

PtSn and Pt_3Sn were evaluated for catalytic activity of the PROX reaction (eq. 1) in H_2 fuel streams, as described in Chapter One. The NPs were loaded onto γ-Al_2O_3 at 1 wt% total metal. Catalysts were initially tested using an inlet gas composition of 1000 ppm CO, 6500 ppm O_2, 49.9% H_2, and balance He.

$$1/2O_2 + H_2 + CO \longrightarrow CO_2 + H_2 \qquad (1)$$

PROX activity decreased in the order of Pt_3Sn > PtSn, represented by decreasing O_2 concentration as a function of temperature (fig. 3-4). It should be noted that O_2 concentrations are measured in lieu of CO and CO_2 due to the following: CO readings are less stable with the current GC protocols before the catalytic light-off temperature, illustrated by a steep decrease in CO concentration; and CO_2 is captured by a saturated $Ca(OH)_2$ solution before injection into the GC to prevent peak overlapping due to longer retention times in comparison to other gaseous species. Catalyst light off-temperatures, indicating occurrence of the H_2 oxidation reaction and increased conversation rates of some reactant gases, are shown by steep decreases in O_2 concentration. Although the O_2 concentration decreases to ~ 0% of the original concentration due to the oxidation of H_2, the diminishing and disappearing CO signal also indicates that PROX is occurring; thus, O_2 is being consumed by the PROX reaction and the oxidation of H_2, the latter of which could potentially be monitored via generated H_2O using different analytical conditions.

The presence of Sn surface atoms combined with a relatively high concentration of Pt surface atoms led Pt_3Sn to display PROX activity beginning at ~95°C. This supports the theory that Pt_3Sn is more PROX active than PtSn. Pt-Sn alloys have shown higher electrochemical catalysis compared to Pt due to the bifunctional mechanism; thus, with this assumption, Pt PROX analysis was not performed.

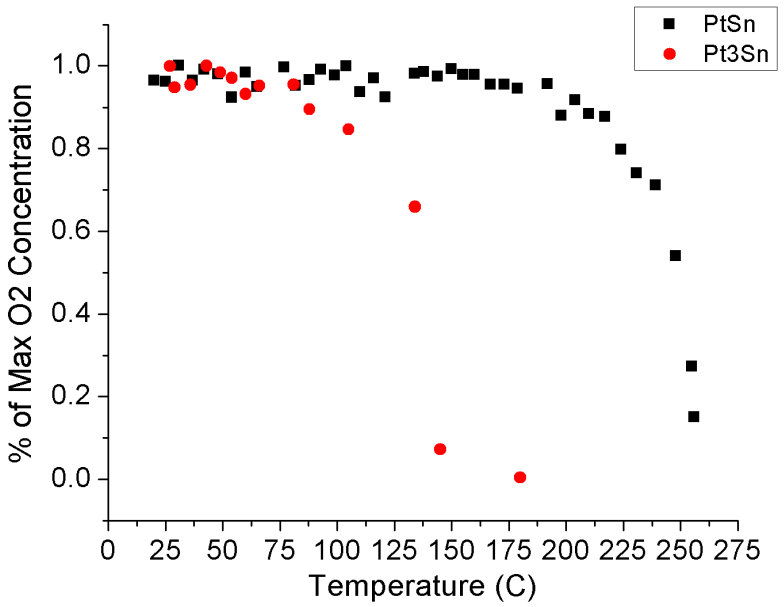

Figure 3-4. PROX activity for PtSn and Pt_3Sn using 1000 ppm CO. O_2 Concentration as a function of temperature shows increased conversion rate at ~95°C for Pt_3Sn and ~225°C for PtSn.

The effects of varying catalytic conditions on Pt_3Sn PROX activity were further investigated. Deviating from the industry-relevant concentration of 1000 ppm CO, gas feeds containing 500 ppm CO and 2000 ppm CO were tested. As expected, PROX activity and H_2 oxidation light-off temperature increased as CO concentration increased (fig. 3-5), attributed to decreasing O_2 concentrations. As O_2 is necessary for the PROX and H_2 oxidation reactions, more consumption of O_2 for PROX will require higher temperatures to make PROX facile and less reliant on O_2, whereby the O_2 can then be utilized for H_2 oxidation. Furthermore, slight concentration and light-off temperature differences were consistently observed in comparison of 1000 ppm CO and 2000 ppm CO data, making this data notable for the study. This catalytic study will be used in further investigations of support effects and variations in O_2 concentration on Pt_3Sn PROX activity.

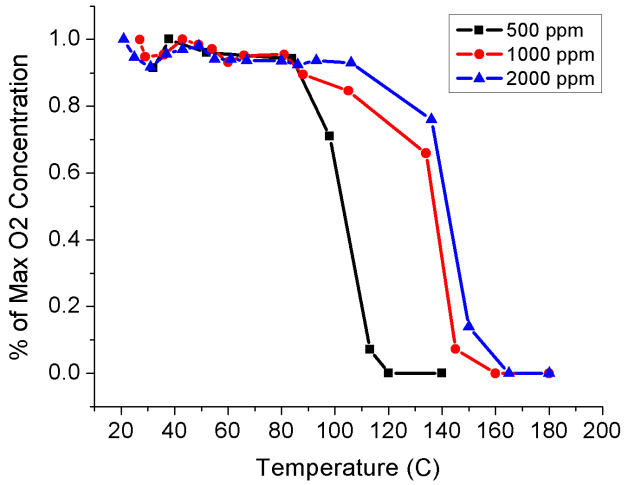

Figure 3-5. PROX activity for Pt_3Sn supported on γ-Al_2O_3 at various CO concentrations, showing increased O_2 conversion rates occurring at lower temperatures for lower CO concentrations.

3.3 Co-Ni Nanoparticles

3.3.1 Synthesis and Characterization

1,2-hexadecanediol polyol reduction using PVP (MW=55,000) as the surfactant in DPE at 255°C was used to synthesize monometallic Co NPs with an average diameter of 5.0 nm, which formed magnetic agglomerates with an average diameter of 51.5 nm. HRTEM was used to confirm Co NPs using EDX for elemental analysis (fig. S25). Polyol reduction in 1,4-butanediol at 235°C with PVP also yielded Co NPs as magnetic agglomerates with an average diameter of 198.4 nm. Powder XRD profile showed the peak at 2θ=46° of the (111) plane of cubic ($Fm\bar{3}m$) Co. The presence of this relatively intense peak supports the formation of cubic Co NPs. Reaction conditions yielding smaller Co NPs and agglomerates were chosen for further Co-Ni experiments.

Three synthetic methods were used to generate Ni NPs. Polyol reduction of $Ni(acac)_2$ in DPE using 1,2-hexadecanediol produced NPs with an average diameter of

9.1 nm. Lattice spacings of ~2.0 Å and XRD analysis both confirmed cubic ($Fm\bar{3}m$) Ni NPs with minimal surface oxide. Polyol reduction in 1,4-butanediol with PVP gave polydisperse NPs with average diameter of 57.8 nm. Lattice fringe analysis showed (111) planes of cubic Ni visible in different geometric structures, including single crystal tetrahedra and twinned particles (fig. 3-6)[106]. 25.0 nm Ni NPs were synthesized by polyol reduction with 1,2-hexadecanediol in octadecene, similar to DPE reaction. Monodisperse, cubic Ni NPs were confirmed by TEM, lattice fringe analysis, and XRD. Similar to Co, the 1,2-hexadecanediol-DPE reaction produced NPs of smallest average diameter, making this the preferred method of monometallic Ni synthesis.

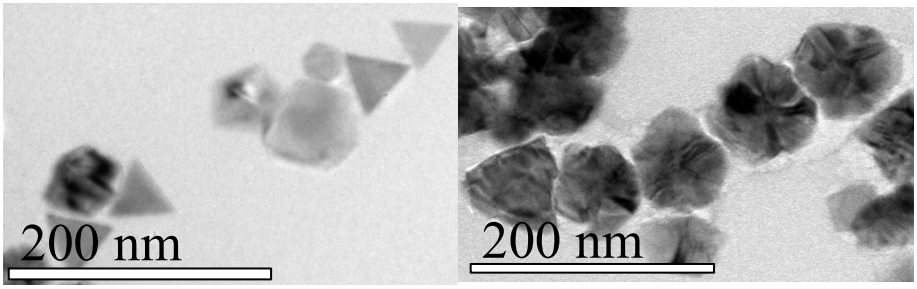

Figure 3-6. TEM images of ~57.8 nm Ni NPs of different geometries (a) Triangular plates of single-crystal Ni NPs (b) Ni NPs exhibiting several instances of twinning.

Co-Ni random alloy NPs were synthesized in anhydrous polyol reduction reactions due to favorable conditions illustrated by Co and Ni monometallic NP syntheses, and the desire to prevent oxide formation. $Co(acac)_2$ and $Ni(acac)_2$ precursors (1:1 molar ratio) in DPE were co-reduced by 1,2-hexadecanediol in the presence of trioctylphosphine, oleic acid, and oleylamine as surfactants.[53,69,89] CoNi NPs were synthesized in distinctive agglomerations. XRD analysis showed a broad peak at 2θ = 44.4°, corresponding to the (111) plane of cubic ($Fm\bar{3}m$) Co-Ni. EDX confirmed bimetallic NP agglomerations with 55 at% Co and 45 at% Ni (fig. S29).

An additional method to CoNi NPs was explored. $Co(acac)_2$ was reduced by 1,2-hexadecanediol with PVP in DPE to generate Co NPs. The Co NP reaction solution was added to $Ni(acac)_2$ and 1,2-hexadecanediol. The mixture was heated to 255°C to induce Ni reduction, and subsequently CoNi alloy NP formation.[53,69,89] CoNi NPs had an average diameter of 27.1 nm. Also, these CoNi NPs did not form agglomerates, allowing for further testing and characterization in contrast to CoNi NPs synthesized in the above procedure. XRD analysis showed a broad peak at $2\theta = 44.4°$, corresponding to the (111) plane of cubic ($Fm\bar{3}m$) Co-Ni. Lattice spacing of ~2.0 Å further confirmed cubic Co-Ni NPs. Lastly, EDX line scan analysis showed even dispersion of Co and Ni across NPs, combining with aforementioned characterization to signify successful synthesis of CoNi NPs.

Co@Ni core-shell NPs were synthesized in a method similar to the second synthesis of CoNi NPs. This modified procedure heated the Co NP and $Ni(acac)_2$ solution to 220°C to produce core-shell architectures with an average inner diameter of 54.3 nm and average shell thickness of 3.0 nm. Similar to the random alloy NPs, the core-shell NPs were magnetic, forming nanowire structures (fig. 3-7). HRTEM lattice fringe analysis showed d-spacings of ~2 Å corresponding to the (111) plane of cubic ($Fm\bar{3}m$) Co and cubic Ni, further confirmed by the peak at $2\theta = 44.4°$ in XRD analysis; similar peak positions for cubic Co and Ni did not aid in distinguishing the core-shell structure. Similar d-spacings of ~2 Å were observed in the core and the shell of the structure (fig. S31), indicative of epitaxial growth. EDX line scans of elemental composition presented varying Co and Ni compositions across the NPs, confirming the core-shell structure (fig. 3-8).

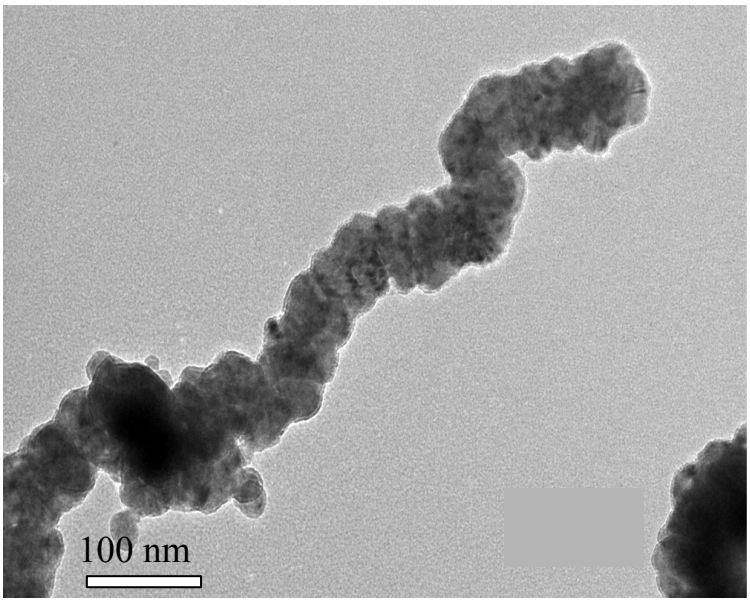

Figure 3-7. TEM of Co@Ni NPs synthesized in DPE using 1,2-hexadecanediol.

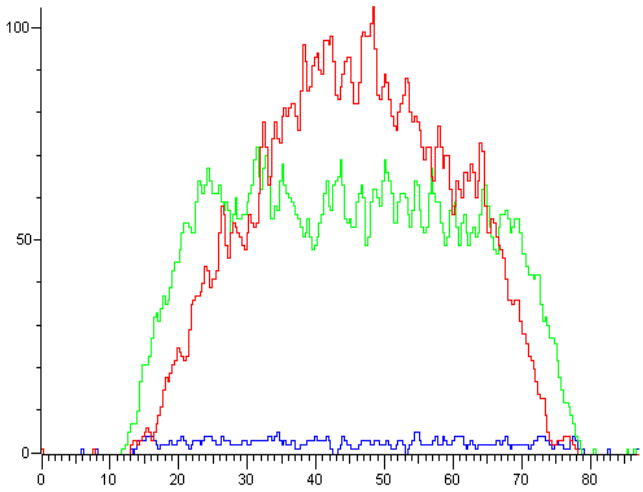

Figure 3-8. EDX line scan data for Co@Ni. Green profile represents Ni, red profile represents Co, and blue profile represents O_2. Lack of near-vertical slope on Co profile edges indicates transmetallation mechanism of NP formation.

The profile of the EDX line scans supports the transmetallation mechanism of NP formation, where Ni atoms replaced some of the outer atoms of the seed Co NPs instead of forming a shell around these outer atoms. Co@Ni core-shell NPs will be compared to Pt_3Sn and other Co-Ni catalysts for PROX activity to investigate viability of the catalyst in terms of cost and activity.

3.4 Conclusion

The work presented herein was performed towards the objective of making and characterizing Pt-Sn and Co-Ni intermetallic and core-shell NPs, and analyzing these systems for catalytic activity. Pt-Sn system NPs have been synthesized, characterized, and evaluated by catalytic studies, showing Pt_3Sn as an effective PROX catalyst. Co-Ni monometallic and bimetallic NPs of different architectures, notably target Co@Ni NPs, have been synthesized and characterized, and will be utilized in future catalytic studies. Aforementioned research was implemented on the basis of theoretical and experimental work presented in the literature.

Bibliography

(1) Hydrogen and Fuel Cells, Department of Energy. http://www1.eere.energy.gov/hydrogenandfuelcells.html (Accessed November 5, 2013).

(2) Basics of Fuel Cells, Department of Energy. http://www1.eere.energy.gov/hydrogenandfuelcells/fuelcells/basics.html (Accessed November 5, 2013).

(3) Natural Gas Reforming, Department of Energy. http://www1.eere.energy.gov/hydrogenandfuelcells/production/natural_gas.html (Accessed November 5, 2013).

(4) Trimm, D., Önsan, Z. Onboard Fuel Conversion for Hydrogen-Fuel-Cell-Driven Vehicles. *Catalysis Reviews*, **2001**, 43, 1-2, 30-84

(5) Larminie, J., Dicks, A., Eds.; *Fuel Cell Systems Explained*; Wiley: England, 2003.

(6) Nilekar, A. U., Alayoglu, S., Eichhorn, B., Mavrikakis, M. Preferential CO Oxidation in Hydrogen: Reactivity of Core−Shell Nanoparticles. *J Am Chem Soc* **2010**, *132*, 7418–7428.

(7) Lu, S., Zhang, C., Liu, Y. Carbon nanotube supported Pt-Ni catalysts for preferential oxidation of CO in hydrogen-rich gases. *Int. J. of Hydrogen Energy* **2011**, *36*, 1939–1948.

(8) Yu, W.; Porosoff, M. D.; Chen, J. G. Review of Pt-Based Bimetallic Catalysis: From Model Surfaces to Supported Catalysts. *Chem Rev* **2012**, *112*, 5780–5817.

(9) Gasteiger, H. A.; Markovic, N. M.; Ross, P. N. Electrooxidation of CO and H2/CO Mixtures on a Well-Characterized Pt3Sn Electrode Surface. *J. Phys. Chem.* **1995**, *99*, 8945–8949.

(10) Greeley, J.; Mavrikakis, M. Near-surface alloys for hydrogen fuel cell applications. *Catal. Today* **2006**, *111*, 52–58.

(11) Hammer, B.; Morikawa, Y.; Norskov, J. K. CO chemisorption at metal surfaces and overlayers. *Phys Rev Lett* **1996**, *76*, 2141–2144.

(12) Xu, Y.; Ruban, A. V.; Mavrikakis, M. Adsorption and Dissociation of O_2 on Pt−Co and Pt−Fe Alloys. *J Am Chem Soc* **2004**, *126*, 4717–4725.

(13) Liu, Z.; Jackson, G. S.; Eichhorn, B. W. Tuning the CO-tolerance of Pt-Fe bimetallic nanoparticle electrocatalysts through architectural control. *Energy Environ. Sci.* **2011**, *4*, 1900–1903.

(14) Mayrhofer, K. J. J.; Juhart, V.; Hartl, K.; Hanzlik, M.; Arenz, M. Adsorbate-induced surface segregation for core-shell nanocatalysts. *Angew. Chem. Int. Ed. Engl.* **2009**, *48*, 3529–3531.

(15) Komatsu, T.; Takasaki, M.; Ozawa, K.; Furukawa, S.; Muramatsu, A. PtCu Intermetallic Compound Supported on Alumina Active for Preferential Oxidation of CO in Hydrogen. *J Phys Chem C* **2013**, *117*, 10483–10491.

(16) Liu, Z.; Jackson, G. S.; Eichhorn, B. W. PtSn intermetallic, core-shell, and alloy nanoparticles as CO-tolerant electrocatalysts for H2 oxidation. *Angew. Chem. Int. Ed. Engl.* **2010**, *49*, 3173–3176.

(17) Watzky, M. A.; Finke, R. G. Transition metal nanocluster formation kinetic and

mechanistic studies. A new mechanism when hydrogen is the reductant: slow, continuous nucleation and fast autocatalytic surface growth. *J Am Chem Soc* **1997**, *119*, 10382–10400.

(18) Aiken, J. D., III; Finke, R. G. A review of modern transition-metal nanoclusters: their synthesis, characterization, and applications in catalysis. *J. Molec. Catal. A* **1999**, *145*, 1–44.

(19) Besson, C.; Finney, E. E.; Finke, R. G. A Mechanism for Transition-Metal Nanoparticle Self-Assembly. *J Am Chem Soc* **2005**, *127*, 8179–8184.

(20) Hornstein, B. J.; Finke, R. G. Transition-Metal Nanocluster Kinetic and Mechanistic Studies Emphasizing Nanocluster Agglomeration: Demonstration of a Kinetic Method That Allows Monitoring of All Three Phases of Nanocluster Formation and Aging. *Chem Mater* **2004**, *16*, 139–150.

(21) Finney, E. E.; Finke, R. G. Nanocluster nucleation and growth kinetic and mechanistic studies: A review emphasizing transition-metal nanoclusters. *J Colloid Interface Sci* **2008**, *317*, 351–374.

(22) Burda, C.; Chen, X.; Narayanan, R.; El-Sayed, M. A. Chemistry and Properties of Nanocrystals of Different Shapes. *Chem Rev* **2005**, *105*, 1025–1102.

(23) Robb, D. T.; Privman, V. Model of Nanocrystal Formation in Solution by Burst Nucleation and Diffusional Growth. *Langmuir* **2008**, *24*, 26–35.

(24) Zhou, S.; Jackson, G. S.; Eichhorn, B. AuPt Alloy Nanoparticles for CO-Tolerant Hydrogen Activation: Architectural Effects in Au-Pt Bimetallic Nanocatalysts. *Adv. Funct. Mater.* **2007**, *17*, 3099–3104.

(25) Alayoglu, S.; Nilekar, A. U.; Mavrikakis, M.; Eichhorn, B. Ru–Pt core–shell nanoparticles for preferential oxidation of carbon monoxide in hydrogen. *Nat Mater* **2008**, *7*, 333–338.

(26) Gasteiger, H. A.; Markovic, N.; Ross, P. N.; Cairns, E. J. Methanol electrooxidation on well-characterized platinum-ruthenium bulk alloys. *J. Phys. Chem.* **1993**, *97*, 12020–12029.

(27) Gurau, B.; Viswanathan, R.; Liu, R.; Lafrenz, T. J.; Ley, K. L.; Smotkin, E. S.; Reddington, E.; Sapienza, A.; Chan, B. C.; Mallouk, T. E.; Sarangapani, S. Structural and Electrochemical Characterization of Binary, Ternary, and Quaternary Platinum Alloy Catalysts for Methanol Electro-oxidation 1. *J Phys Chem B* **1998**, *102*, 9997–10003.

(28) Arico, A. S.; Antonucci, V.; Giordano, N.; Shukla, A. K.; Ravikumar, M. K.; Roy, A.; Barman, S. R.; Sarma, D. D. Methanol oxidation on carbon-supported platinum-tin electrodes in sulfuric acid. *J. Power Sources* **1994**, *50*, 295–309.

(29) Igarashi, H.; Fujino, T.; Zhu, Y.; Uchida, H.; Watanabe, M. CO Tolerance of Pt alloy electrocatalysts for polymer electrolyte fuel cells and the detoxification mechanism. *Phys. Chem. Chem. Phys.* **2001**, *3*, 306–314.

(30) Hammer, B.; Norskov, J. Why Gold is the Noblest of all the Metals. *Nature* **1995**, *376*, 238–240.

(31) Hammer, B.; Norskov, J. Electronic factors determining the reactivity of metal surfaces. *Surf Sci* **1995**, *343*, 211–220.

(32) Ruban, A.; Hammer, B.; Stoltze, P.; Skriver, H. L.; Nørskov, J. K. Surface electronic structure and reactivity of transition and noble metals. *J. Molec. Catal. A* **1997**, *115*, 421–429.

(33) Greeley, J.; Mavrikakis, M. Alloy catalysts designed from first principles. *Nat Mater* **2004**, *3*, 810–815.
(34) Norskov, J. K.; Abild-Pedersen, F.; Studt, F.; Bligaard, T. Surface Chemistry Special Feature: Density functional theory in surface chemistry and catalysis. *Proc. Nat. Acad. Sci.* **2011**, *108*, 937–943.
(35) Greeley, J.; Stephens, I. E. L.; Bondarenko, A. S.; Johansson, T. P.; Hansen, H. A.; Jaramillo, T. F.; Rossmeisl, J.; Chorkendorff, I.; Norskov, J. K. nchem.367. *Nat Chem* **2009**, *1*, 552–556.
(36) Rossmeisl, J.; Ferrin, P.; Tritsaris, G. A.; Nilekar, A. U.; Koh, S.; Bae, S. E.; Brankovic, S. R.; Strasser, P.; Mavrikakis, M. Bifunctional anode catalysts for direct methanol fuel cells. *Energy Environ. Sci.* **2012**, *5*, 8335.
(37) Gasteiger, H. A.; Markovic, N. M.; Ross, P. N. H2 and CO Electrooxidation on Well-Characterized Pt, Ru, and Pt-Ru. 2. Rotating Disk Electrode Studies of CO/H2 Mixtures at 62 .degree.C. *J. Phys. Chem.* **1995**, *99*, 16757–16767.
(38) Gasteiger, H. A.; Markovic, N.; Ross, P. N., Jr; Cairns, E. J. Carbon monoxide electrooxidation on well-characterized platinum-ruthenium alloys. *J. Phys. Chem.* **1994**, *98*, 617–625.
(39) Liu, Z.; Reed, D.; Kwon, G.; Shamsuzzoha, M.; Nikles, D. E. Pt3Sn Nanoparticles with Controlled Size: High-Temperature Synthesis and Room-Temperature Catalytic Activation for Electrochemical Methanol Oxidation. *J Phys Chem C* **2007**, *111*, 14223–14229.
(40) Wang, X.; Altmann, L.; Stöver, J.; Zielasek, V.; Bäumer, M.; Al-Shamery, K.; Borchert, H.; Parisi, J.; Kolny-Olesiak, J. Pt/Sn Intermetallic, Core/Shell and Alloy Nanoparticles: Colloidal Synthesis and Structural Control. *Chem Mater* **2013**, *25*, 1400–1407.
(41) Kwak, J. H.; Hu, J.; Mei, D.; Yi, C. W.; Kim, D. H.; Peden, C. H. F.; Allard, L. F.; Szanyi, J. Coordinatively Unsaturated Al3+ Centers as Binding Sites for Active Catalyst Phases of Platinum on -Al2O3. *Science* **2009**, *325*, 1670–1673.
(42) Small, M. W.; Sanchez, S. I.; Marinkovic, N. S.; Frenkel, A. I.; Nuzzo, R. G. Influence of Adsorbates on the Electronic Structure, Bond Strain, and Thermal Properties of an Alumina-Supported Pt Catalyst. *ACS Nano* **2012**, *6*, 5583–5595.
(43) Lee, A. F.; Wilson, K.; Lambert, R. M. Structure and stability of the platinum/aluminium interface: alloying and substrate vacancy formation on Pt {111}/Al. *Surf Sci* **2000**, *446*, 145–152.
(44) Ojeda, M.; Nabar, R.; Nilekar, A. U.; Ishikawa, A.; Mavrikakis, M.; Iglesia, E. CO activation pathways and the mechanism of Fischer–Tropsch synthesis. *J. Catal.* **2010**, *272*, 287–297.
(45) Khodakov, A. Y.; Chu, W.; Fongarland, P. Advances in the Development of Novel Cobalt Fischer−Tropsch Catalysts for Synthesis of Long-Chain Hydrocarbons and Clean Fuels. *Chem Rev* **2007**, *107*, 1692–1744.
(46) Chu, W.; Chernavskii, P.; Gengembre, L.; Pankina, G.; Fongarland, P.; Khodakov, A. Cobalt species in promoted cobalt alumina-supported Fischer–Tropsch catalysts. *J. Catal.* **2007**, *252*, 215–230.
(47) Cook, K. M.; Poudyal, S.; Miller, J. T.; Bartholomew, C. H.; Hecker, W. C. Reducibility of alumina-supported cobalt Fischer–Tropsch catalysts: Effects of

noble metal type, distribution, retention, chemical state, bonding, and influence on cobalt crystallite size. *Appl. Catal. A* **2012**, *449*, 69–80.

(48) Lu, S.; Lonergan, W. W.; Bosco, J. P.; Wang, S.; Zhu, Y.; Xie, Y.; Chen, J. G. Low temperature hydrogenation of benzene and cyclohexene: A comparative study between γ-Al2O3 supported PtCo and PtNi bimetallic catalysts. *J. Catal.* **2008**, *259*, 260–268.

(49) Alexeev, O. S.; Gates, B. C. Supported Bimetallic Cluster Catalysts. *Ind. Eng. Chem. Res.* **2003**, *42*, 1571–1587.

(50) Keaton, R. J.; Blacquiere, J. M.; Baker, R. T. Base Metal Catalyzed Dehydrogenation of Ammonia−Borane for Chemical Hydrogen Storage. *J Am Chem Soc* **2007**, *129*, 1844–1845.

(51) Burghgraef, H.; Jansen, A.; van Santen, R. A. Methane activation and dehydrogenation on nickel and cobalt: a computational study. *Surf Sci* **1995**, *324*, 345–356.

(52) Sinfelt, J. Catalytic hydrogenolysis and dehydrogenation over copper-nickel alloys. *J. Catal.* **1972**, *24*, 283–296.

(53) Sharma, S.; Gajbhiye, N. S.; Ningthoujam, R. S. Synthesis and self-assembly of monodisperse CoxNi100-x (x=50,80) colloidal nanoparticles by homogenous nucleation. *J Colloid Interface Sci* **2010**, *351*, 323–329.

(54) Zhang, J.; Wang, H.; Xi, C.; Shakouri, M.; Hu, Y.; Dalai, A. K. Design and Preparation of Ni-Co Bimetallic Nanocatalyst for Carbon Dioxide Reforming of Methane. In *ACS Symposium Series*; American Chemical Society: Washington, DC, 2012; Vol. 1092, pp. 195–221.

(55) Yamauchi, T.; Tsukahara, Y.; Yamada, K.; Sakata, T.; Wada, Y. Nucleation and Growth of Magnetic Ni−Co (Core−Shell) Nanoparticles in a One-Pot Reaction under Microwave Irradiation. *Chem Mater* **2011**, *23*, 75–84.

(56) Panday, S.; Daniel, B. S. S.; Jeevanandam, P. Synthesis of nanocrystalline Co–Ni alloys by precursor approach and studies on their magnetic properties. *J. Magn. Magn. Mater.* **2011**, *323*, 2271–2280.

(57) Liu, G.; Gao, P.-X. A review of NOx storage/reduction catalysts: mechanism, materials and degradation studies. *Catal. Sci. Technol.* **2011**, *1*, 552.

(58) Granger, P.; Parvulescu, V. I. Catalytic NO xAbatement Systems for Mobile Sources: From Three-Way to Lean Burn after-Treatment Technologies. *Chem Rev* **2011**, *111*, 3155–3207.

(59) Zhou, S.; Varughese, B.; Eichhorn, B.; Jackson, G.; McIlwrath, K. Pt-Cu core-shell and alloy nanoparticles for heterogeneous NO(x) reduction: anomalous stability and reactivity of a core-shell nanostructure. *Angew. Chem. Int. Ed. Engl.* **2005**, *44*, 4539–4543.

(60) Auvray, X.; Pingel, T.; Olsson, E.; Olsson, L. The effect gas composition during thermal aging on the dispersion and NO oxidation activity over Pt/Al2O3 catalysts. *Appl. Catal. B* **2013**, *129*, 517–527.

(61) Gómez-García, M. A.; Pitchon, V.; Kiennemann, A. Pollution by nitrogen oxides: an approach to NOx abatement by using sorbing catalytic materials. *Environment International* **2005**, *31*, 445–467.

(62) Matam, S. K.; Kondratenko, E. V.; Aguirre, M. H.; Hug, P.; Rentsch, D.; Winkler, A.; Weidenkaff, A.; Ferri, D. The impact of aging environment on the

evolution of Al2O3 supported Pt nanoparticles and their NO oxidation activity. *Appl. Catal. B* **2013**, *129*, 214–224.

(63) Hansgen, D. A.; Vlachos, D. G.; Chen, J. G. nchem.626. *Nat Chem* **2010**, *2*, 484–489.

(64) Schüth, F.; Palkovits, R.; Schlögl, R.; Su, D. S. Ammonia as a possible element in an energy infrastructure: catalysts for ammonia decomposition. *Energy Environ. Sci.* **2012**, *5*, 6278.

(65) Karim, A. M.; Prasad, V.; Mpourmpakis, G.; Lonergan, W. W.; Frenkel, A. I.; Chen, J. G.; Vlachos, D. G. Correlating Particle Size and Shape of Supported Ru/γ-Al 2O 3Catalysts with NH 3Decomposition Activity. *J Am Chem Soc* **2009**, *131*, 12230–12239.

(66) Zhang, J.; Xu, H.; Li, W. Kinetic study of NH3 decomposition over Ni nanoparticles: The role of La promoter, structure sensitivity and compensation effect. *"Appl. Catal. A* **2005**, *296*, 257–267.

(67) Bock, C.; Paquet, C.; Couillard, M.; Botton, G. A.; MacDougall, B. R. Size-selected synthesis of PtRu nano-catalysts: reaction and size control mechanism. *J Am Chem Soc* **2004**, *126*, 8028–8037.

(68) Park, J.; Joo, J.; Kwon, S. G.; Jang, Y.; Hyeon, T. Synthesis of Monodisperse Spherical Nanocrystals. *Angew. Chem. Int. Ed.* **2007**, *46*, 4630–4660.

(69) Gajbhiye, N. S.; Sharma, S.; Nigam, A. K.; Ningthoujam, R. S. Tuning of single to multi-domain behavior for monodispersed ferromagnetic cobalt nanoparticles. *Chem. Phys. Lett.* **2008**, *466*, 181–185.

(70) Bönnemann, H.; Richards, R. M. Nanoscopic Metal Particles. Synthetic Methods and Potential Applications. *Eur. J. Inorg. Chem.* **2001**.

(71) Nilekar, A. U.; Sasaki, K.; Farberow, C. A.; Adzic, R. R.; Mavrikakis, M. Mixed-metal Pt monolayer electrocatalysts with improved CO tolerance. *J Am Chem Soc* **2011**, *133*, 18574–18576.

(72) Sun, S.; Murray, C. B. Synthesis of monodisperse cobalt nanocrystals and their assembly into magnetic superlattices (invited). *J. Appl. Phys.* **1999**, *85*, 4325–4330.

(73) B nnemann, H.; Brinkmann, R.; Neiteler, P. Preparation and catalytic properties of NR4+-stabilized palladium colloids. *Appl. Organomet. Chem.* **1994**, *8*, 361–378.

(74) Bönnemann, H.; Braun, G.; Brijoux, W.; Brinkmann, R.; Tilling, A. S.; Seevogel, K.; Siepen, K. Nanoscale colloidal metals and alloys stabilized by solvents and surfactants Preparation and use as catalyst precursors. *J. Organomet. Chem.* **1996**, *520*, 143–162.

(75) Kao, M. J.; Tien, D. C.; Jwo, C. S.; Tsung, T. T. The study of hydrophilic characteristics of ethylene glycol. *J. Phys.: Conf. Ser.* **2005**, *13*, 442–445.

(76) Fan, F.-R.; Liu, D.-Y.; Wu, Y.-F.; Duan, S.; Xie, Z.-X.; Jiang, Z.-Y.; Tian, Z.-Q. Epitaxial Growth of Heterogeneous Metal Nanocrystals: From Gold Nano-octahedra to Palladium and Silver Nanocubes. *J Am Chem Soc* **2008**, *130*, 6949–6951.

(77) Zhang, J.; Tang, Y.; Lee, K.; Ouyang, M. Nonepitaxial Growth of Hybrid Core-Shell Nanostructures with Large Lattice Mismatches. *Science* **2010**, *327*, 1634–1638.

(78) Wang, G.; Wu, H.; Wexler, D.; Liu, H.; Savadogo, O. Ni@ Pt core–shell nanoparticles with enhanced catalytic activity for oxygen reduction reaction. *J. Alloys Compd.* **2010**, *503*, L1–L4.

(79) Liu, Z.; Hu, J. E.; Wang, Q.; Gaskell, K.; Frenkel, A. I.; Jackson, G. S.; Eichhorn, B. PtMo Alloy and MoO x@Pt Core−Shell Nanoparticles as Highly CO-Tolerant Electrocatalysts. *J Am Chem Soc* **2009**, *131*, 6924–6925.

(80) Characterization of Superparamagnetic "Core−Shell" Nanoparticles and Monitoring Their Anisotropic Phase Transition to Ferromagnetic 'Solid Solution' Nanoalloys. *J Am Chem Soc* **2001**, *123*, 5743–5746.

(81) Park, J.-I.; Kim, M. G.; Jun, Y.-W.; Lee, J. S.; Lee, W.-R.; Cheon, J. Characterization of Superparamagnetic "Core−Shell" Nanoparticles and Monitoring Their Anisotropic Phase Transition to Ferromagnetic 'Solid Solution' Nanoalloys. *J Am Chem Soc* **2004**, *126*, 9072–9078.

(82) Andersson, K. J.; Calle-Vallejo, F.; Rossmeisl, J.; Chorkendorff, I. Adsorption-Driven Surface Segregation of the Less Reactive Alloy Component. *J. Am. Chem. Soc.* **2009**, *131*, 2404–2407.

(83) Tao, F.; Grass, M. E.; Zhang, Y.; Butcher, D. R.; Aksoy, F.; Aloni, S.; Altoe, V.; Alayoglu, S.; Renzas, J. R.; Tsung, C.-K.; Zhu, Z.; Liu, Z.; Salmeron, M.; Somorjai, G. A. Evolution of Structure and Chemistry of Bimetallic Nanoparticle Catalysts under Reaction Conditions. *J. Am. Chem. Soc.* **2010**, *132*, 8697–8703.

(84) Chee, S. S.; Lee, J. H. Effects of pH on Tin Nanoparticles Prepared Using a Modified Polyol Synthesis. *Appl. Mech. Mat.* **2013**.

(85) CHEE, S.-S.; LEE, J.-H. Reduction synthesis of tin nanoparticles using various precursors and melting behavior. *Electron. Mater. Lett.* **2012**, *8*, 587–593.

(86) Balan, L.; Schneider, R.; Billaud, D.; Ghanbaja, J. A new organometallic synthesis of size-controlled tin(0) nanoparticles. *Nanotechnology* **2005**, *16*, 1153–1158.

(87) Özkar, S.; Finke, R. G. Nanocluster Formation and Stabilization Fundamental Studies: Ranking Commonly Employed Anionic Stabilizers via the Development, Then Application, of Five Comparative Criteria. *J. Am. Chem. Soc.* **2002**, *124*, 5796–5810.

(88) Ott, L. S.; Finke, R. G. Transition-metal nanocluster stabilization for catalysis: A critical review of ranking methods and putative stabilizers. *Coord. Chem. Rev.* **2007**, *251*, 1075–1100.

(89) Carenco, S.; Boissière, C.; Nicole, L.; Sanchez, C.; Le Floch, P.; Mézailles, N. Controlled Design of Size-Tunable Monodisperse Nickel Nanoparticles. *Chem. Mater.* **2010**, *22*, 1340–1349.

(90) Park, J. Y.; Aliaga, C.; Renzas, J. R.; Lee, H.; Somorjai, G. A. The Role of Organic Capping Layers of Platinum Nanoparticles in Catalytic Activity of CO Oxidation. *Catal. Lett.* **2009**, *129*, 1–6.

(91) Li, D.; Wang, C.; Tripkovic, D.; Sun, S.; Markovic, N. M.; Stamenkovic, V. R. Surfactant Removal for Colloidal Nanoparticles from Solution Synthesis: The Effect on Catalytic Performance. *ACS Catal* **2012**, *2*, 1358–1362.

(92) Rabis, A.; Rodriguez, P.; Schmidt, T. J. Electrocatalysis for Polymer Electrolyte Fuel Cells: Recent Achievements and Future Challenges. *ACS Catal*

2012, *2*, 864–890.
(93) Zhang, S.; Yuan, X.-Z.; Hin, J. N. C.; Wang, H.; Friedrich, K. A.; Schulze, M. A review of platinum-based catalyst layer degradation in proton exchange membrane fuel cells. *J. Power Sources* **2009**, *194*, 588–600.
(94) Debe, M. K. nature11115. *Nature* **2012**, *486*, 43–51.
(95) Zhang, S.; Shao, Y.; Liao, H.; Engelhard, M. H.; Yin, G.; Lin, Y. Polyelectrolyte-Induced Reduction of Exfoliated Graphite Oxide: A Facile Route to Synthesis of Soluble Graphene Nanosheets. *ACS Nano* **2011**, *5*, 1785–1791.
(96) Antolini, E. Carbon supports for low-temperature fuel cell catalysts. *Appl. Catal. B* **2009**, *88*, 1–24.
(97) Imran Jafri, R.; Rajalakshmi, N.; Ramaprabhu, S. Nitrogen doped graphene nanoplatelets as catalyst support for oxygen reduction reaction in proton exchange membrane fuel cell. *J. Mater. Chem.* **2010**, *20*, 7114.
(98) Sinkler, W.; Bradley, S. A.; Ziese, U.; Jong, K. 3D-TEM Study of Gamma Alumina Catalyst Supports. *MAM* **2006**, *12*, 52.
(99) An, K.; Alayoglu, S.; Musselwhite, N.; Plamthottam, S.; Melaet, G.; Lindeman, A. E.; Somorjai, G. A. Enhanced CO Oxidation Rates at the Interface of Mesoporous Oxides and Pt Nanoparticles. *J. Am. Chem. Soc.* **2013**, *135*, 16689–16696.
(100) Alayoglu, S.; Zavalij, P.; Eichhorn, B.; Wang, Q.; Frenkel, A. I.; Chupas, P. Structural and Architectural Evaluation of Bimetallic Nanoparticles: A Case Study of Pt−Ru Core−Shell and Alloy Nanoparticles. *ACS Nano* **2009**, *3*, 3127–3137.
(101) Andersson, M.; Paradis, H.; Yuan, J.; Sundén, B. Review of catalyst materials and catalytic steam reforming reactions in SOFC anodes. *Int. J. of Energy Res.* **2011**.
(102) Ghosh Chaudhuri, R.; Paria, S. Core/shell nanoparticles: classes, properties, synthesis mechanisms, characterization, and applications. *Chem. Rev.* **2012**, *112*, 2373–2433.
(103) Boudart, M.; McDonald, M. A. Structure sensitivity of hydrocarbon synthesis from carbon monoxide and hydrogen. *J. Phys. Chem.* **1984**, *88*, 2185–2195.
(104) Flaherty, D. W.; Yu, W.-Y.; Pozun, Z. D.; Henkelman, G.; Mullins, C. B. Mechanism for the water-gas shift reaction on monofunctional platinum and cause of catalyst deactivation. *J. Catal.* **2011**, *282*, 278–288.
(105) Rioux, R. M.; Song, H.; Hoefelmeyer, J. D.; Yang, P.; Somorjai, G. A. High-Surface-Area Catalyst Design: Synthesis, Characterization, and Reaction Studies of Platinum Nanoparticles in Mesoporous SBA-15 Silica. *J. Phys. Chem. B* **2005**, *109*, 2192–2202.
(106) Xia, Y.; Xiong, Y.; Lim, B.; Skrabalak, S. E. Shape-Controlled Synthesis of Metal Nanocrystals: Simple Chemistry Meets Complex Physics *Angew. Chem. Int. Ed.* **2008**, *48*, 60–103.
(107) Lattimer, W.; *The Oxidation States of the Elements and their Potentials in Aqueous Solutions*; Prentice Hall: New York, 1952.
(108) Inorganic Crystal Structure Database